Acta Crystallographica Section D
Biological Crystallography
ISSN 1399-0047

Structural and biochemical characterization of MdaB from cariogenic *Streptococcus mutans* reveals an NADPH-specific quinone oxidoreductase

Zixi Wang,[a]* Lanfen Li,[a] Yu-Hui Dong[b] and Xiao-Dong Su[a]*

[a]State Key Laboratory of Protein and Plant Gene Research, and Biodynamic Optical Imaging Center (BIOPIC), Peking University, Beijing 100871, People's Republic of China, and [b]Beijing Synchrotron Radiation Facility, Institute of High Energy Physics, Chinese Academy of Sciences, Beijing 100049, People's Republic of China

Correspondence e-mail: wangzixi08@gmail.com, xdsu@pku.edu.cn

Received 3 February 2013
Accepted 13 December 2013

PDB references: SmMdaB–$NADP^+$, 3lcm; SmMdaB–menadione, 4f8y

The *smu*.1420 gene from the cariogenic pathogen *Streptococcus mutans* encodes a putative protein which has sequence homology to NQO [NAD(P)H:quinone oxidoreductase] family members, including mammalian NQO and bacterial MdaB (modulator of drug activity B). NQO can detoxify quinones by converting them to hydroquinones and prevent the generation of reactive oxygen species. Thus, comprehensive studies on Smu.1420 will be important for uncovering the antioxidation and antidrug mechanisms of *S. mutans*. Here, the catalytic properties of Smu.1420 have been characterized, and its structure was determined in complexes with $NADP^+$ and menadione, respectively. Smu.1420 binds menadione directly and exhibits a pronounced preference for NADPH over NADH as a substrate, demonstrating that it is an NADPH-specific quinone oxidoreductase. The structure of Smu.1420 shows a compact homodimer with two substrate pockets located in the cleft of the dimer interface. The nicotinamide moiety of $NADP^+$ is bound on top of the isoalloxazine moiety of the FAD cofactor and overlaps with the binding site of menadione, suggesting a hydride-transfer process from NADPH to FAD and then to menadione. Two strongly basic patches near the substrate pocket are expected to confer the preference for NADPH over NADH. These studies shed light on future drug development against the cariogenic pathogen *S. mutans*.

1. Introduction

The NAD(P)H:quinone oxidoreductase (NQO) protein family is evolutionarily conserved from bacteria to humans. The proteins usually contain a FAD cofactor, form a physiological homodimer and catalyze a two-electron transfer process from NAD(P)H to quinones (Li *et al.*, 1995; Tedeschi *et al.*, 1995; Zhao *et al.*, 1997; Foster *et al.*, 1999). Quinones, such as ubiquinone-8 and menaquinone-8, function as membrane-associated electron carriers and transport hydrogen and electrons between respiratory-protein complexes in bacteria (Georgellis *et al.*, 2001). Although these quinones are essential for the respiratory chain, they can also divert the electron flow away and cause oxidative stress in cells (Hayashi *et al.*, 1990; Adams & Jia, 2005, 2006). Among these quinones, menadione (vitamin K_3, a metabolic intermediate of menaquinone) is usually used as a model quinone in cell cultures and other investigations to elevate the levels of peroxide and superoxide radical in cells. NQO plays an important role in the detoxification of these quinones by diverting them from the one-electron reduction products semiquinones, which can react with oxygen molecules spontaneously and result in lipid peroxidation and depletion of cellular reductants such as

reduced glutathione (Kwiek *et al.*, 2004; Tedeschi *et al.*, 1995; Beyer *et al.*, 1997; Li *et al.*, 1995).

The structure and function of mammalian NQO proteins have been extensively investigated. Two homologous NQOs are found in mammals, named NQO1 (or DT-diaphorase; QR1) and NQO2 (or QR2). NQO1 is composed of a major α/β catalytic domain and a small C-terminal domain (Li *et al.*, 1995), whereas NQO2 lacks the C-terminal domain but binds a zinc ion in the C-terminal region that is expected to participate in electron transfer during catalysis (Foster *et al.*, 1999). The catalytic properties of the two enzymes are also different. NQO1 utilizes NADH and NADPH as substrates at a similar rate (Tedeschi *et al.*, 1995), whereas NQO2 prefers nonphosphorylated ribosyl, alkyl or phenyl dihydronicotinamides as substrates (Zhao *et al.*, 1997; Foster *et al.*, 1999; Chen *et al.*, 2000). Despite these differences, both enzymes can transfer two electrons to a quinone, preventing the generation of the semiquinone as well as reactive oxygen species.

Although mammalian NQO homologues are widely distributed in bacteria, as indicated by a *BLAST* search, only those of *Escherichia coli* and *Helicobacter* have been investigated. The *E. coli* NQO homologue was initially found to be a menadione-induced enzyme that could partially alleviate the toxicity of menadione (Hayashi *et al.*, 1990). Further studies showed that overexpression of the *E. coli* NQO homologue imparted resistance towards several drugs such as DMP840 and adriamycin, and therefore bacterial NQO homologues have also been named modulator of drug activity B (MdaB; Chatterjee & Sternberg, 1995). MdaB mutants in the microaerophilic pathogens *H. pylori* and *H. hepaticus* have been shown to be more sensitive to the oxygen level and oxidative reagents such as H_2O_2 and organic hydroperoxide, resulting in decreased viability and colonization (Wang & Maier, 2004; Hong *et al.*, 2008). To date, from bacteria, only the structure of *E. coli* MdaB has been well documented (Adams & Jia, 2006). It is a single-domain FAD-binding protein and does not bind zinc ion like mammalian NQO2 (Adams & Jia, 2006). Although numerous structures of mammalian NQO1 and NQO2 in complex with substrates and xenobiotics have been determined, how the structurally different bacterial MdaBs select substrates and catalyze the electron-transfer process remains elusive owing to the lack of enzyme–substrate complex structures.

In this study, we purified and characterized the MdaB protein (Smu.1420) from *Streptococcus mutans*, a pathogen that plays a key role in tooth decay (Ajdić *et al.*, 2002). An enzymatic assay showed that Smu.1420 (named SmMdaB in this paper) has a pronounced preference for NADPH over NADH as a substrate. Spectroscopic measurements support this result and confirm the direct binding of menadione to the substrate pocket. We have determined both the SmMdaB–$NADP^+$ and the SmMdaB–menadione complex structures to 1.8 Å resolution, which reveal that the binding sites of menadione and the nicotinamide moiety of $NADP^+$ overlap and are adjacent to the isoalloxazine ring of FAD. The complex structures also provide an explanation for the substrate specificity towards NADPH. Furthermore, through structural comparison and multiple sequence alignments, we have uncovered the mechanisms of how the mammalian NQO and bacterial MdaB select FAD rather than FMN as a cofactor. These results shed light on the antioxidation and antidrug mechanisms of the cariogenic pathogen *S. mutans* and provide a structural basis for future drug development.

Table 1
Data-collection and refinement statistics.

Values in parentheses are for the highest resolution shell.

	SmMdaB–$NADP^+$	SmMdaB–menadione
Data collection		
Space group	$P2_1$	$P2_1$
Unit-cell parameters		
a (Å)	50.60	50.61
b (Å)	79.12	79.41
c (Å)	106.28	106.50
$\alpha = \gamma$ (°)	90	90
β (°)	90.01	90.08
Resolution (Å)	50.0–1.80 (1.83–1.80)	20.0–1.80 (1.84–1.80)
$R_{\rm merge}$† (%)	7.6 (30.5)	12.0 (32.5)
$\langle I/\sigma(I)\rangle$	30.5 (4.3)	18.5 (6.3)
Completeness (%)	95.4 (92.3)	98.6 (89.2)
Multiplicity	3.5 (3.2)	6.6 (4.4)
Unique reflections	73792	77264
Refinement		
$R_{\rm work}$‡/$R_{\rm free}$§ (%)	16.0/18.8	15.6/18.3
No. of atoms		
Protein	6044	6144
Ligand	265	264
Water	371	558
B factors (Å^2)		
Protein	21.6	18.6
Ligand	23.9	20.2
Water	23.2	20.6
R.m.s. deviations		
Bond lengths (Å)	0.006	0.006
Bond angles (°)	1.0	1.1
Ramachandran plot		
Most favourable (%)	88.7	87.6
Additionally allowed (%)	10.6	11.3
Generously allowed (%)	0.1	0.6
Disallowed (%)	0.6	0.6

† $R_{\rm merge} = \sum_{hkl}\sum_i |I_i(hkl) - \langle I(hkl)\rangle| / \sum_{hkl}\sum_i I_i(hkl)$. ‡ $R_{\rm work} = \sum_{hkl} ||F_{\rm obs}| - |F_{\rm calc}|| / \sum_{hkl} |F_{\rm obs}|$. § $R_{\rm free} = \sum_{hkl} ||F_{\rm obs}| - |F_{\rm calc}|| / \sum_{hkl} |F_{\rm obs}|$. The $R_{\rm free}$ value was calculated from a randomly selected 5% of reflections that were not used in the refinement.

2. Materials and methods

2.1. Protein expression, purification and lysine methylation

The *smu.1420* gene was amplified from the genomic DNA of *S. mutans* UA159 and subsequently cloned into pET-21b vector (Novagen) with a C-terminal His tag. The plasmid was transformed into *E. coli* BL21(DE3) strain and the protein was expressed at 18°C overnight by induction with 1 m*M* β-D-thiogalactopyranoside (IPTG). The harvested cells were suspended in buffer *A* (500 m*M* NaCl, 20 m*M* Tris–HCl pH 7.5) and lysed by sonication. After centrifugation, the supernatant was loaded into a HiTrap Ni^{2+}-affinity column (GE Healthcare) equilibrated with buffer *A*. The column was washed with 20% buffer *B* (500 m*M* NaCl, 500 m*M* imidazole, 20 m*M* Tris–HCl pH 7.5) and the target protein was eluted with a gradient to 80% buffer *B*. The protein was further

purified by gel filtration using a Superdex 75 column (GE Healthcare) in buffer *C* (200 m*M* NaCl, 20 m*M* Tris–HCl pH 7.5) and concentrated to approximately 25 mg ml^{-1}. To generate lysine-methylated protein for enzymatic assay, the purified protein was first exchanged into buffer *D* (200 m*M* NaCl, 50 m*M* HEPES pH 7.5) using a desalting column (GE Healthcare). Lysine methylation was performed as described previously (Walter *et al.*, 2006).

2.2. Crystallization

To obtain crystals of the SmMdaB–NADP$^+$ complex, NADPH tetrasodium salt (Roche) was dissolved in buffer *C* and added to the protein to final concentrations of 5 m*M* NADPH and 0.7 m*M* protein. Owing to the rapid oxidation of NADPH by the protein, the ligand in the crystal should be NADP$^+$. To obtain crystals of the SmMdaB–menadione complex, menadione (Sigma) was added to buffer *C* and sonicated to homogeneity. The homogeneous menadione solution was rapidly added to the protein and mixed thoroughly, with final concentrations of 5 m*M* menadione and 0.7 m*M* protein. Crystal screening was carried out by the sitting-drop vapour-diffusion method at 18°C by mixing 1 µl protein solution and 1 µl reservoir solution. Crystal Screen, Crystal Screen 2, Index and Natrix kits (Hampton Research, a total of 240 conditions) were used for initial screening. Both

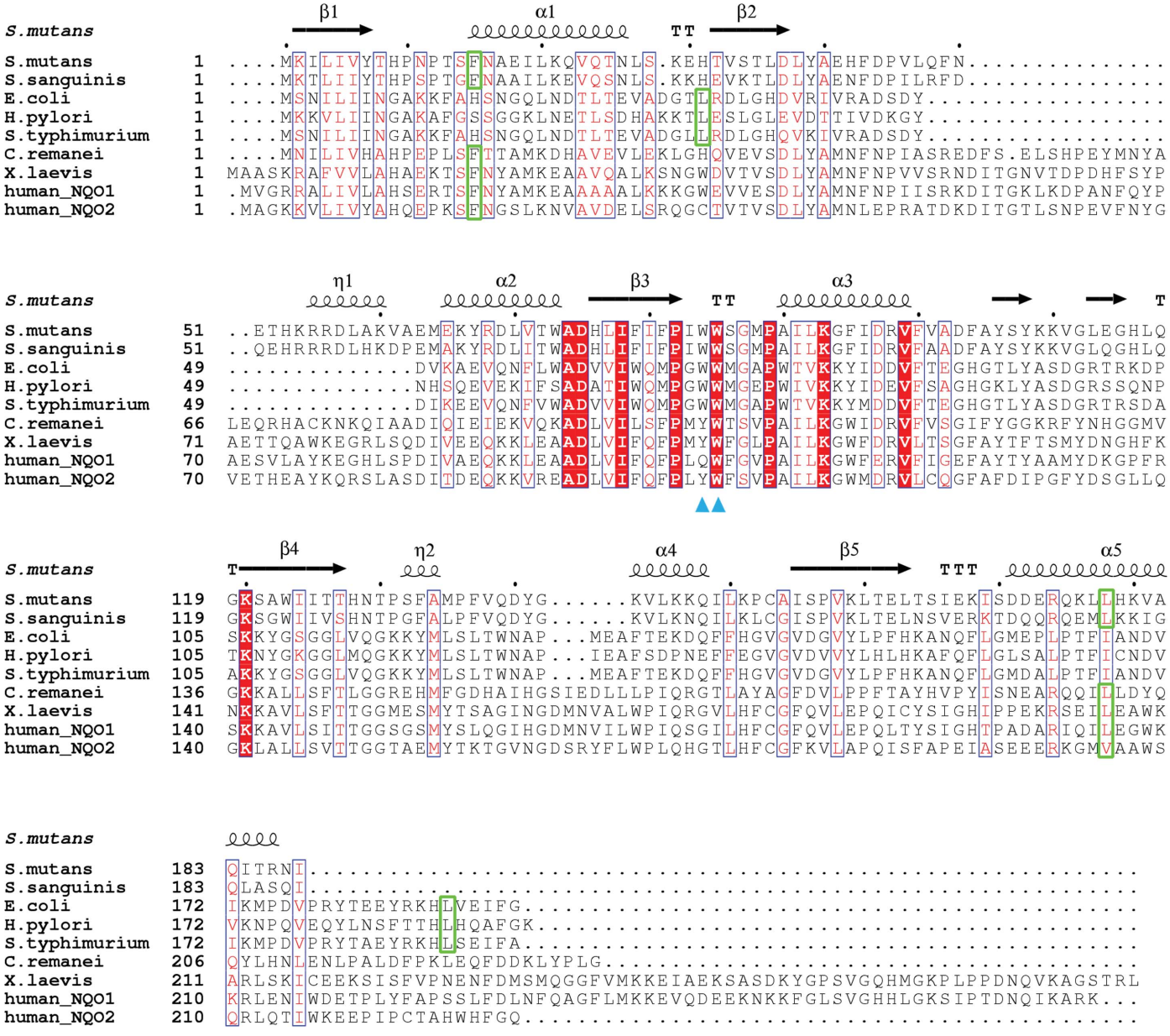

Figure 1
Multiple sequence alignment of *S. mutans* MdaB (UniProtKB accession code Q8DTD1) with eight other homologous proteins. The SmMdaB homologues are from *Streptococcus sanguinis* (F9E3J5), *Escherichia coli* (P0AEY5), *Helicobacter pylori* (E6S218), *Salmonella typhimurium* (E8XBA7), *Caenorhabditis remanei* (E3NTC2), *Xenopus laevis* (A5D8M8) and *Homo sapiens* (NQO1, P15559; NQO2, P16083). Key residues interacting with the isoalloxazine ring of FAD are marked with blue triangles. Key residues involved in binding the adenine moiety of FAD are boxed in green rectangles.

complex crystals appeared using a solution consisting of 200 m*M* KCl, 50 m*M* HEPES pH 7.5, 35%(*v*/*v*) pentaerythritol propoxylate (5/4 PO/OH) after 2 d.

2.3. Data collection and structural determination

Before data collection, the crystals were soaked for 1–2 min in reservoir solution supplemented with 20% glycerol and were then flash-cooled in liquid nitrogen. Both data sets were collected at −173°C. The SmMdaB–NADP$^+$ data set was collected on beamline 1W2B at Beijing Synchrotron Radiation Facility (BSRF) using a MAR555 flat-panel detector. The SmMdaB–menadione data set was collected on beamline BL17A at the Photon Factory, KEK, Japan using an ADSC Quantum 315r CCD detector. Both data sets were integrated and scaled using the *HKL*-2000 package (Otwinowski & Minor, 1997) and were assigned to space group $P2_1$. As the β angle is very close to 90° (Table 1), the data sets were also processed in space group $P222_1$. The SmMdaB–NADP$^+$ data sets in space groups $P2_1$ and $P222_1$ were both used in molecular replacement with human NQO2 (PDB entry 1zx1; Structural Genomics Consortium, unpublished work) as the search model using *MOLREP* (Vagin & Teplyakov, 2010). The phases could be determined using the $P2_1$ data set but not with the $P222_1$ data set, which is very likely to be owing to a high twinning fraction of the data as detected by *phenix.xtriage* (Adams *et al.*, 2002). The structure was further manually built using *Coot* (Emsley & Cowtan, 2004) and refined using *phenix.refine* (Adams *et al.*, 2002) with the twin operator (*h*, −*k*, −*l*) added during the refinement. The SmMdaB–menadione structure was solved by molecular replacement using the SmMdaB–NADP$^+$ structure as the initial model and was refined using a similar procedure. Data-collection and refinement statistics are summarized in Table 1. The four residues in the disallowed region of the Ramachandran plot in both structures are Asp140 in the four protein chains from one asymmetric unit. These residues have well defined electron density.

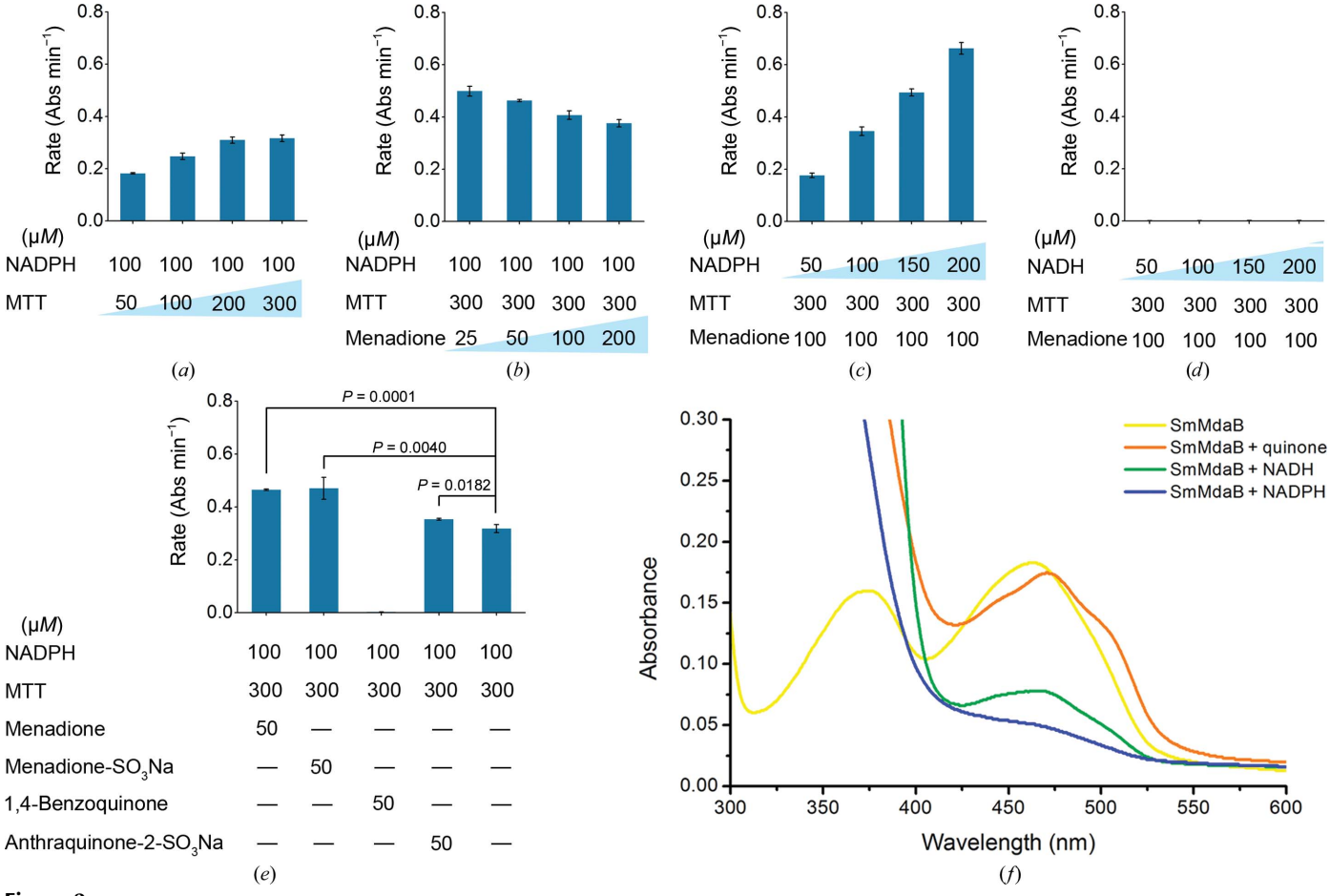

Figure 2
Enzymatic assays and electronic absorption spectroscopy. (*a*) The catalytic rate is shown with a fixed concentration of NADPH (100 μ*M*) and varying concentrations of MTT (50–300 μ*M*). (*b*) The catalytic rate is shown with fixed concentrations of NADPH (100 μ*M*) and MTT (300 μ*M*) and varying concentrations of menadione (25–200 μ*M*). (*c*) The catalytic rate is shown with fixed concentrations of MTT (300 μ*M*) and menadione (100 μ*M*) and varying concentrations of NADPH (50–200 μ*M*). (*d*) The catalytic rate is shown with fixed concentrations of MTT (300 μ*M*) and menadione (100 μ*M*) and varying concentrations of NADH (50–200 μ*M*). (*e*) The catalytic rate is shown using menadione, menadione sodium bisulfite, 1,4-benzoquinone and sodium anthraquinone-2-sulfonate as electron acceptors. Data are represented as the mean ± standard deviation of three repeats. *P* values were calculated using Student's *t*-test. (*f*) Electronic absorption spectroscopic analysis of SmMdaB in the native state, the menadione-binding state and the reduced state using NADPH and NADH as electron donors. The spectral data for buffer *C* were used as a baseline.

2.4. Enzymatic assays

Enzymatic assays were performed using a UV-2450 spectrophotometer (Shimadzu) at room temperature. NADPH tetrasodium salt and 3-(4,5-dimethylthiazol-2-yl)-2,5-diphenyltetrazolium bromide (MTT) were each dissolved in H_2O, and menadione, menadione sodium bisulfite, 1,4-benzoquinone and sodium anthraquinone-2-sulfonate were each dissolved in dimethyl sulfoxide (DMSO) as stocks. The reaction buffer consisted of 200 m*M* NaCl, 20 m*M* Tris–HCl, 0.01% Tween 20, 0.2 mg ml^{-1} BSA pH 7.5. In a total 1 ml reaction system, the indicated concentrations of substrates were added and the reaction was started by the addition of recombinant protein to a final concentration of 200 n*M*. The reduced product of MTT was continuously monitored at 578 nm. Each measurement was repeated three times.

2.5. Electronic absorption spectroscopy

Electronic absorption spectroscopy was also performed using a UV-2450 spectrophotometer at room temperature. 0.25 m*M* protein in buffer *C*, or 0.25 m*M* protein mixed with either 0.5 m*M* menadione, 1 m*M* NADPH or 1 m*M* NADH, was placed in a 1 ml quartz cuvette. Electronic absorption spectra were collected over the range 300–600 nm with 0.2 nm data-point intervals. The spectral data for buffer *C* were used as a baseline.

2.6. Analytical ultracentrifugation

Analytical ultracentrifugation measurements were performed using a ProteomeLab XL-I (Beckman Coulter) analytical ultracentrifuge with an An-60 Ti rotor. The protein in buffer *C* was centrifuged at a speed of 60 000 rev min^{-1} (262 000*g*) for 6 h at 25°C.

3. Results

3.1. Smu.1420 (SmMdaB) is an NADPH-specific quinone oxidoreductase

The Smu.1420 protein was annotated as a putative oxidoreductase after sequencing of the *S. mutans* genome (Ajdić *et al.*, 2002). It has a flavodoxin-like fold (PF02525) according to the Pfam database (Bateman *et al.*, 2004). Using a *BLAST* search of the UniProt Knowledgebase, we found that Smu.1420 has dramatic homology to mammalian NQO and *E. coli* MdaB (Fig. 1). Thus, Smu.1420 may be the MdaB protein in *S. mutans*. Given the sequence conservation of the aligned homologous proteins (Fig. 1), we speculate that Smu.1420 (named SmMdaB in this study) is an NAD(P)H: quinone oxidoreductase.

We cloned and purified full-length SmMdaB and measured its enzymatic activities using different electron donors and acceptors. According to previously reported methods (Winger *et al.*, 2009; Wu *et al.*, 1997), the enzymatic reduction of the substrate menadione to menadiol is coupled to the reduction of MTT, which results in an increased absorbance at 570–590 nm. Interestingly, we found that MTT itself could be a substrate of SmMdaB and be reduced by NADPH (Fig. 2*a*). With the addition of menadione to the reaction system, the catalytic rate increased further, suggesting that menadione is also reduced by SmMdaB (Fig. 2*b*). However, on an increase in menadione the measured rate decreased, probably owing to a complex substrate-competition and redox reaction mechanism (Fig. 2*b*). The catalytic rate increased rapidly with increasing NADPH concentrations (Fig. 2*c*), but was almost undetectable when NADPH was substituted by NADH (Fig. 2*d*). To test whether other quinones could be a substrate of SmMdaB, we substituted menadione with menadione sodium bisulfite, 1,4-benzoquinone or sodium anthraquinone-2-sulfonate in the system. We found that SmMdaB had a low catalytic rate towards anthraquinone-2-sulfonate compared with menadione and menadione sodium bisulfite (Fig. 2*e*). In contrast, 1,4-benzoquinone almost totally blocked the enzymatic activity (Fig. 2*e*). These results demonstrate that SmMdaB is an NADPH-specific quinone oxidoreductase and prefers menadione as the substrate, which is in accordance with the catalytic properties of previously characterized bacterial MdaBs (Wang & Maier, 2004; Hong *et al.*, 2008; Hayashi *et al.*, 1996).

3.2. The spectrum of SmMdaB in different states

The catalytic properties of SmMdaB were further demonstrated by monitoring the absorbance spectrum of the protein in different states (Fig. 2*f*). The protein purified with an intense yellow colour, and alone it had absorbance peaks at 375 and 463 nm, which are characteristic of an oxidized flavin cofactor. Upon addition of menadione, the absorption bands were perturbed. The second absorption peak of the oxidized protein shifted to 471 nm and two shoulders were observed at approximately 440 and 500 nm, suggesting direct binding of menadione to the active site of SmMdaB.

Addition of NADPH and NADH both caused a decrease in absorption at 463 nm (Fig. 2*f*), which was a result of flavin reduction. Although the catalytic rate towards NADH was almost undetectable, it could still reduce the protein, probably because NADH is an analogue of NADPH and excess NADH was added and incubated with the protein. However, NADH was not well utilized as a substrate, as supported by the observation that in the presence of excess NADH a small portion of the protein was still maintained oxidized, as indicated by a peak at 463 nm (Fig. 2*f*). These observations are in agreement with the results of the enzymatic assays.

3.3. Overall structure of SmMdaB

To elucidate the catalytic mechanisms, we crystallized SmMdaB in the presence of NADPH and menadione, respectively. Both crystals diffracted to 1.8 Å resolution and belonged to space group $P2_1$. The phases were determined by molecular replacement using the human NQO2 structure (PDB entry 1zx1) as a search model. The SmMdaB–NADP$^+$ and SmMdaB–menadione structures were refined to R_{work} and R_{free} values of 16.0 and 18.8% and of 15.6 and 18.3%,

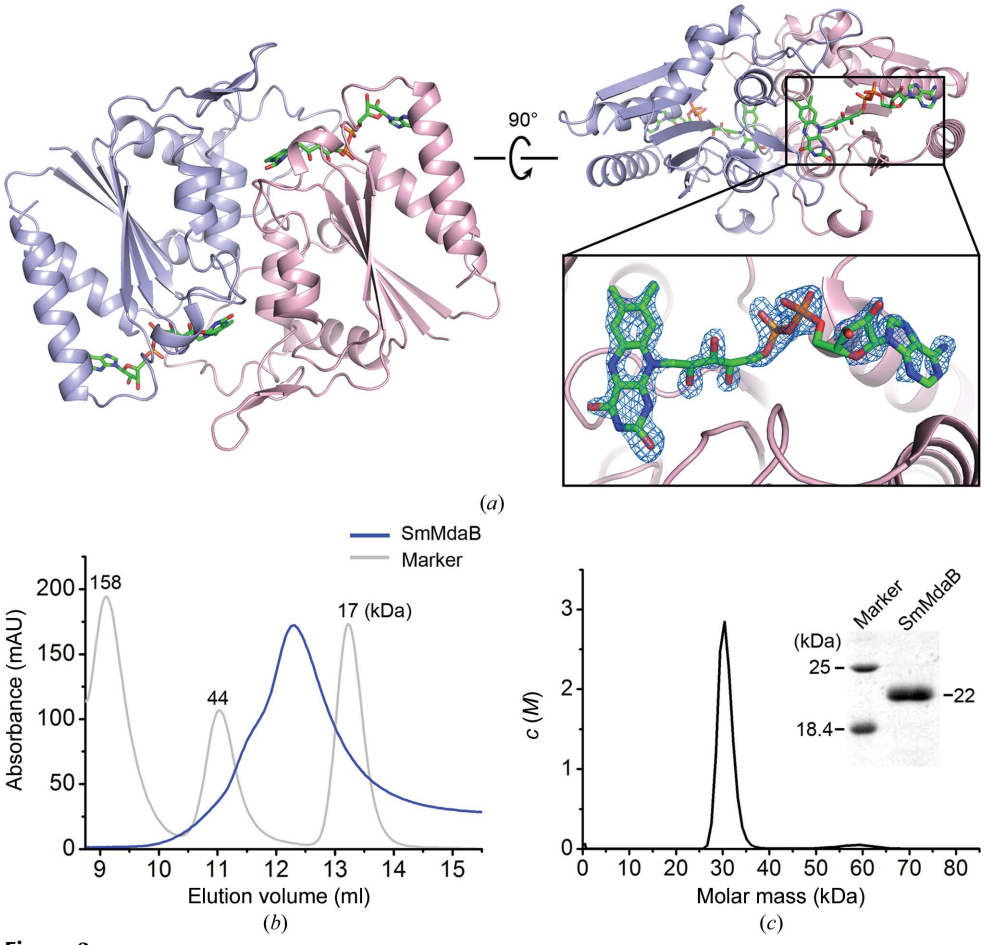

Figure 3
Overall structure of SmMdaB and its oligomeric state in solution. (*a*) SmMdaB exists as a homodimer in the crystals. FAD (coloured green) binds on top of each sandwich-like monomer structure. The $F_o - F_c$ electron-density map (contoured at 3.0σ) calculated with the FAD molecule removed is shown as a blue mesh over the refined model. (*b*) Gel-filtration analysis showed that SmMdaB elutes as a wide peak that spans the expected dimer and monomer volumes. (*c*) Ultracentrifugation analysis shows that SmMdaB has a molecular weight of 30.6 ± 1.6 kDa in solution, which is intermediate between a monomer (22 kDa) and a dimer (44 kDa) as indicated by SDS–PAGE.

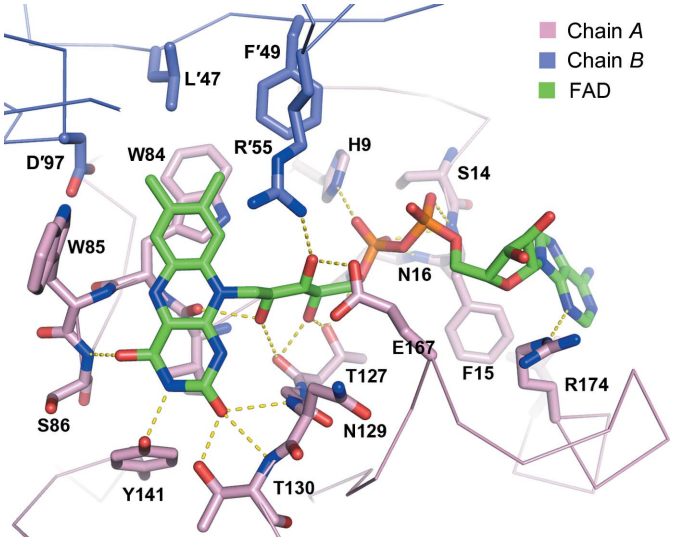

Figure 4
Interactions between FAD and the protein. Hydrogen bonds are shown as yellow dashed lines.

respectively. Each asymmetric unit contained two noncrystallographic homodimeric proteins.

Resembling other NQO family members, the overall structure of the SmMdaB monomer is a canonical α–β–α sandwich structure, with five parallel β-strands (named β1–β5) forming a sheet in the centre surrounded by five α-helices (named α1–α5) on both sides (Fig. 3*a*). Electron density for FAD was clearly observed at the top of the sandwich structure, and the FAD molecule was easily built (Fig. 3*a*). Dimerization leads to the formation of the two active sites per dimer around the isoalloxazine ring of FAD, which are located in the cleft of the dimer interface.

Analysis showed that dimerization was mediated by extensive mixed hydrogen bonds and hydrophobic interactions, with a rather large buried area of 1428 Å^2. Unexpectedly, the dimer structure in solution was not as stable as other characterized NQO family members, as indicated by gel-filtration and ultracentrifugation analyses. Gel-filtration results showed that SmMdaB eluted as a wide peak spanning the expected dimer and monomer volumes (Fig. 3*b*). Ultracentrifugation demonstrated that the protein had a molecular weight of 30.6 ± 1.6 kDa in solution, a weight approximately intermediate between a monomer (22 kDa) and a dimer (44 kDa) (Fig. 3*c*). These observations suggest that SmMdaB exists in an equilibrium between rapid association and disassociation processes in solution.

3.4. Structural basis for FAD recognition

The isoalloxazine ring of FAD is mainly stabilized by two contiguous tryptophan residues (Trp84 and Trp85) through π–π stacking (Fig. 4). These two tryptophan residues are well conserved among bacterial MdaBs, whereas the first tryptophan is usually replaced by tyrosine with maintained aromaticity in many animal species (Fig. 1). Hydrogen-bonding interactions with the O2, O4 and N3 atoms of the isoalloxazine ring also contribute to the binding. The ribitol and pyrophosphate moieties of FAD interact with the protein through extensive hydrogen bonds to maintain an extended

conformation, but no direct interaction was observed between the ribose moiety and the protein (Fig. 4).

The interaction with the adenine ring of FAD is of great interest as it may confer the preference of NQO family proteins for FAD binding rather than FMN binding. In the presented structures of the NQO family (Figs. 5*a*–5*d*), two residues from the α1 and α5 helices form a hydrophobic pocket that plays a key role in binding the adenine ring of FAD. In the structure of SmMdaB, the adenine-binding pocket is formed by the hydrophobic Phe15 from the α1 helix and Leu178 from the α5 helix (Fig. 5*a*). The phenylalanine residue in the α1 helix is also conserved in human NQO1 and NQO2, whereas the other residue from the α5 helix is substituted by Leu204 and Val204, respectively, with retained hydrophobicity (Figs. 5*b* and 5*c*). In *E. coli* MdaB, the pocket interacting with the adenine ring is composed of Leu31 and Val188, which are also two hydrophobic residues (Fig. 5*d*). In addition, the adenine ring of FAD in SmMdaB, human NQO1 and NQO2 was further stabilized by hydrogen-bonding interactions (Figs. 5*a*–5*c*), whereas that in *E. coli* MdaB was stabilized by an amino–aromatic interaction (Burley & Petsko, 1986) with the side chain of Gln30 (Fig. 5*d*). Importantly, the conformation of helices α1 and α5 in these four structures is generally the same (Figs. 5*a*–5*d*).

In contrast, observations on the FMN-binding protein YhdA from *Bacillus subtilis* show that it bears no structural features of the adenine-binding pocket, although this enzyme possesses a similar flavodoxin-like fold and catalyzes a similar electron-transfer process from NADPH to an azo dye (Fig. 5*e*; Binter *et al.*, 2009). The N-terminus of the α1 helix in YhdA contains no hydrophobic residues for adenine binding. The α5 helix in YhdA protrudes away from the α1 helix and therefore cannot provide the other hydrophobic residue to form the adenine-binding pocket. Furthermore, the loop between the β5 strand and the α5 helix in *B. subtilis* YhdA is much longer than the corresponding regions in NQO family proteins. This extended loop in YhdA blocks the binding of the adenosine moiety of FAD and allows YhdA to utilize FMN as its cofactor.

3.5. Structure of the SmMdaB–NADP$^+$ complex

To determine how SmMdaB specifically selects NADPH as an electron donor, we crystallized the protein in the presence

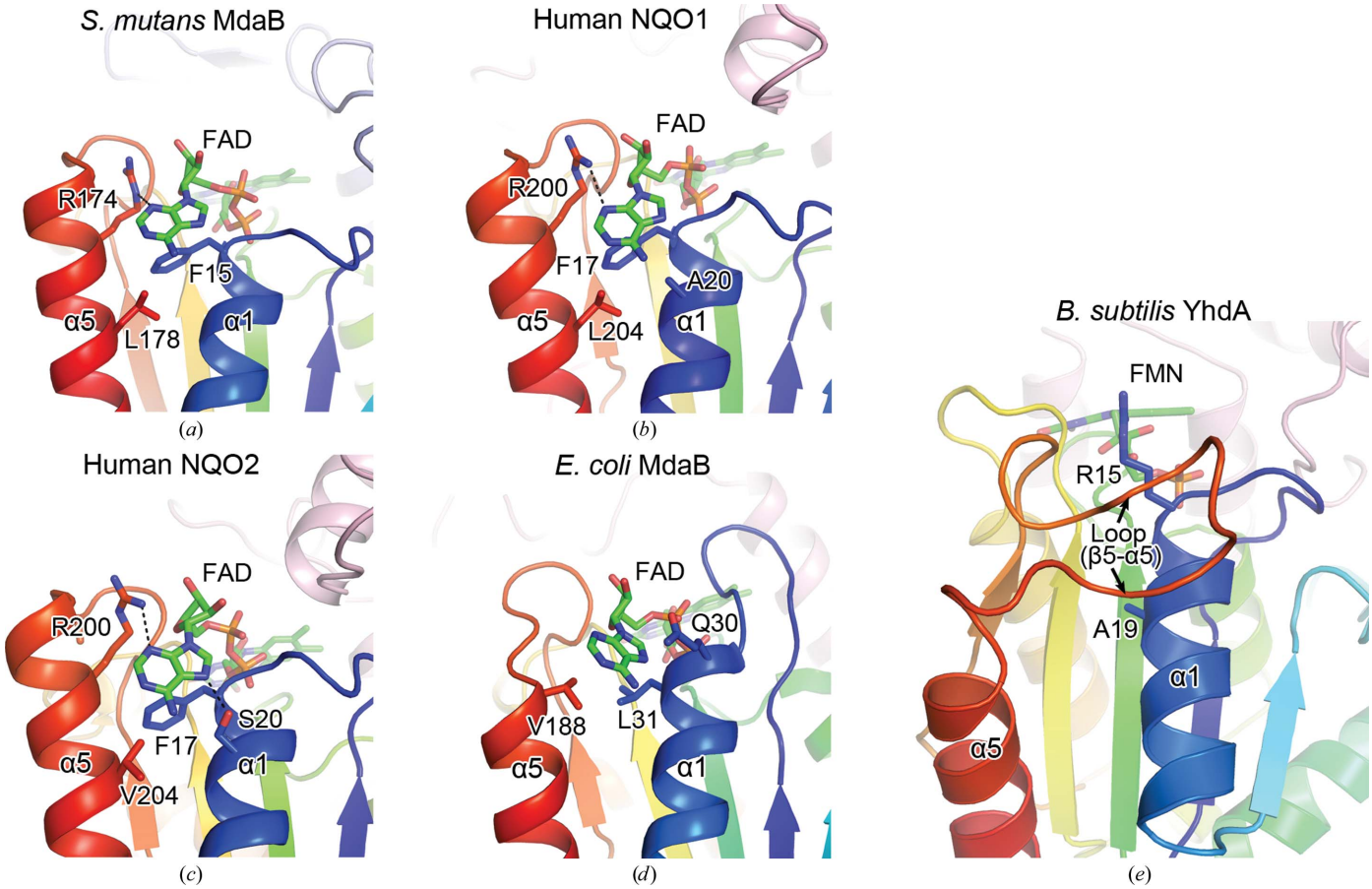

Figure 5
Structural basis for FAD recognition. In the structures of SmMdaB (*a*), human NQO1 (*b*), human NQO2 (*c*) and *E. coli* MdaB (*d*), two relatively conserved hydrophobic residues from the α1 and α5 helices form a hydrophobic pocket to bind the adenine moiety of FAD. The two hydrophobic residues for adenine binding are Phe15 and Leu178 in SmMdaB, Phe17 and Leu204 in human NQO1, Phe17 and Val204 in human NQO2, and Leu31 and Val188 in *E. coli* MdaB. (*e*) *B. subtilis* Yhda, a protein with a similar flavodoxin-like fold, does not bear any of the structural features of the adenine-binding pocket. It binds an FMN molecule as a cofactor. The five structures are coloured as a rainbow (from blue at the N-terminus to red at the C-terminus) and are presented in a view centred on the tail of the FAD or FMN cofactor.

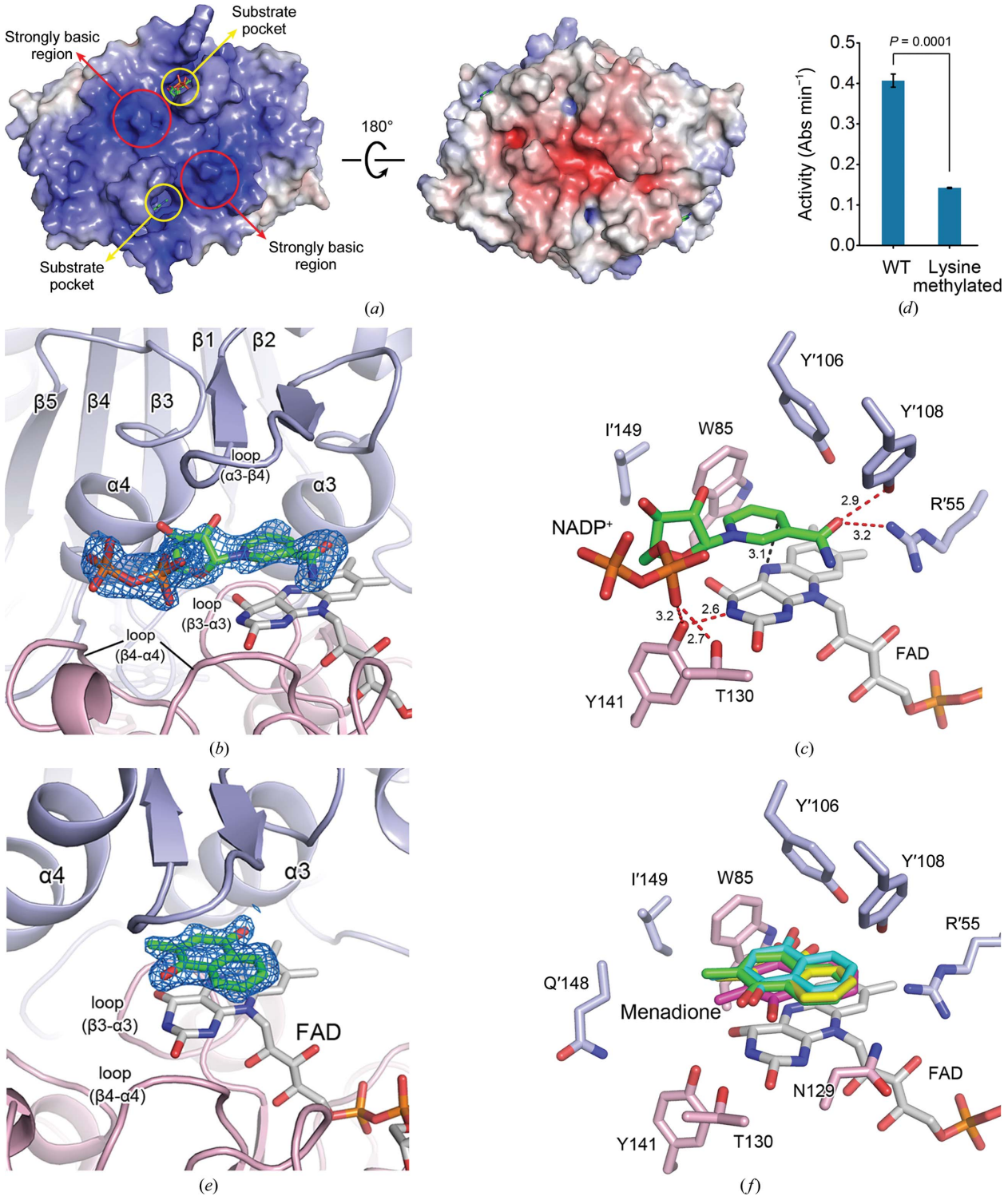

Figure 6
Structures of the complexes of SmMdaB with NADP$^+$ and menadione. (*a*) Electrostatic surface of the homodimeric protein. The orientation of the surface presentation is the same as in the left structure in Fig. 3(*a*). Two distinct prominent surface patches were observed, one of which was basic and the other of which was weakly acidic. The substrate pockets open to the basic patch. Two strongly basic regions were found near the substrate pocket, which were expected to interact with the 2′-phosphate of NADPH and determine NADPH as the preferred substrate. (*b*) The $2F_o - F_c$ electron-density map (contoured at 1.0σ) is shown over the partially built NADP$^+$ molecule. (*c*) Detailed interactions between the protein and NADP$^+$ are shown. Hydrogen bonds are marked as red dashed lines with bond lengths shown in angstroms. The distance between the electron-donor C atom in the nicotinamide moiety and the electron-acceptor N atom in FAD is 3.1 Å (shown as a black dashed line). (*d*) Comparison of the enzymatic activities of wild-type (WT) and lysine-methylated proteins. The assay system consisted of 100 µ*M* NADPH, 100 µ*M* menadione, 300 µ*M* MTT and 200 n*M* WT or lysine-methylated protein. Data were represented as the mean ± standard deviation of three repeats. (*e*) The $2F_o - F_c$ electron-density map (contoured at 1.0σ) is shown over the menadione molecule. (*f*) The protein binds menadione mainly through hydrophobic interactions. The four SmMdaB–menadione monomer structures in one asymmetric are superimposed and the menadione molecules are shown.

of excess NADPH. As demonstrated by the spectral analysis, the added NADPH was rapidly oxidized by the enzyme, resulting in the reduction of FAD. However, the reduced FAD was gradually re-oxidized, probably by oxygen molecules, and the nearly colourless protein solution after the addition of NADPH returned to its original yellow colour in less than half an hour, implying depletion of NADPH. Therefore, the molecule co-crystallized is expected to be $NADP^+$.

Before the analysis of the protein–$NADP^+$ interaction, we first generated an electrostatic surface of the protein and examined the environment of the substrate pocket (Fig. 6*a*). The protein shows two distinct prominent surface patches, one of which is basic and the other of which is weakly acidic. The two substrate pockets in a homodimer protein open to the basic surface patch, which may determine the substrate properties.

In the refined model, none of the four $NADP^+$ molecules in the asymmetric unit was fully built owing to incompleteness of the electron density. For one of the $NADP^+$ molecules, the nicotinamide in the head and the ribose and pyrophosphate group in the middle were built, but not the AMP moiety in the tail (Fig. 6*b*). For the other three $NADP^+$ molecules in the asymmetric unit only the nicotinamide head was built. Structural analysis shows that a phenylalanine residue (Phe133) from an adjacent molecule protrudes above the $NADP^+$ binding pocket, which sterically hinders the binding of the AMP tail (Supplementary Fig. S1[1]). The nicotinamide moiety stacks parallel to the isoalloxazine ring of FAD, with a distance of 3.1 Å between the electron-donor C atom in nicotinamide and the electron-acceptor N atom in FAD (Fig. 6*c*). The side chains of three residues, Trp85 and Tyr′106 and Tyr′108 from the neighbouring monomer in the SmMdaB homodimer, form the back and the top of the active site. They interact with and stabilize the nicotinamide ring mainly through hydrophobic interactions. The side chains of Arg′55 and Tyr′108 from the neighbouring monomer form two hydrogen bonds to the nicotinamide ring which may contribute to the orientation of the substrate. In addition, two hydrogen-bonded interactions are formed between the protein and one O atom of the pyrophosphate group of $NADP^+$ (Fig. 6*c*).

Because electron density for the AMP moiety of $NADP^+$ was not observed, structural information on how the protein interacts with the 2′-phosphate of AMP and selects NADPH as the substrate is not known. However, observations from the electrostatic surface should explain the substrate preference for NADPH but not NADH. Three positively charged residues (Lys146, Lys147 and Lys151) in each monomer constitute a strongly basic region near the substrate pocket. This region is very likely to interact with the 2′-phosphate of NADPH and determines NADPH as the preferred substrate. To support this hypothesis, we generated lysine-methylated SmMdaB and measured the enzymatic activity using NADPH as an electron donor, since mutation of the three lysine residues resulted in a great loss in protein solubility. As predicted, lysine methylation markedly compromised the catalytic ability of SmMdaB, probably owing to weakened binding to the 2′-phosphate of NADPH (Fig. 6*d*).

3.6. Structure of the SmMdaB–menadione complex

Compared with the SmMdaB–$NADP^+$ complex, the active-site conformation of the SmMdaB–menadione structure is very similar. Electron density for menadione is clearly observed on top of the isoalloxazine ring of FAD (Fig. 6*e*). The menadione stacks parallel to the isoalloxazine of FAD and forms extensive hydrophobic interactions with surrounding aromatic residues, including Trp85, Tyr′106 and Tyr′108 (Fig. 6*f*). The menadione has the same binding site as the nicotinamide moiety of NADPH, suggesting a hydride-transfer process from NADPH to FAD and then to menadione. When the four protein monomer structures in one asymmetric unit are superimposed, it can be seen that the conformation of the four menadione molecules is generally the same (Fig. 6*f*). The distances between the O atom on the C1 of menadione and N5 on the isoalloxazine of FAD range from 3.4 to 3.9 Å, which are suitable distances for hydride transfer.

4. Discussion

SmMdaB was overexpressed in *E. coli* and purified as a natural FAD-binding protein. Although no additional FAD molecules were supplemented during cell culture and crystallization, the protein and crystals showed an intense yellow colour and electron density for FAD was clearly observed, suggesting that FAD was tightly bound to the protein. A small faction of the SmMdaB protein without FAD binding (indicated by a rather weakened colour and an identical molecular weight on SDS–PAGE) was eluted at the void volume by gel filtration and defied crystallization, probably owing to oligomerization of the protein. In contrast, the *E. coli* MdaB protein could be crystallized in the absence of FAD (Adams & Jia, 2006). The behavioural difference of the two proteins can probably be attributed to the different conformation and residue composition of the loop connecting the β1 strand and the α1 helix (Supplementary Fig. S2). This loop is relatively hydrophilic in *E. coli* MdaB and probably covers the hydrophobic FAD binding site when FAD is absent, whereas in SmMdaB it is short and protrudes away from the FAD binding site, thus resulting in the exposure of a large hydrophobic area in the absence of FAD.

Compared with *E. coli* MdaB, the structure of SmMdaB is more similar to that of human NQO2. The r.m.s.d. value between SmMdaB and human NQO2 (PDB entry 1zx1) is 2.0 Å (185 C^α atoms aligned), whereas that between SmMdaB and *E. coli* NQO2 (PDB entry 2b3d; Adams & Jia, 2006) is 2.3–2.4 Å (166 C^α atoms aligned) according to the *DALI* server (Holm & Rosenström, 2010). As shown in the sequence alignment, the loop region between the β2 strand and the α2 helix, which participates in intermolecular interactions within the homodimer, is longer in the Gram-positive *Streptococcus*

[1] Supporting information has been deposited in the IUCr electronic archive (Reference: XB5071).

MdaB and animal NQO than in the aligned Gram-negative bacterial MdaB (Fig. 1). Furthermore, the two hydrophobic residues involved in adenine moiety binding in *Streptococcus* MdaB align well with those of animal NQO but not with the Gram-negative bacterial MdaB (Fig. 1). In addition, given the sequence conservation (Fig. 1), we expect that other uncharacterized NQO family members will be FAD-binding proteins rather than FMN-binding protein.

Enzymatic assays demonstrate that SmMdaB has a pronounced preference for NADPH over NADH as a substrate. This is also true for other characterized MdaBs in bacteria (Wang & Maier, 2004; Hong *et al.*, 2008; Hayashi *et al.*, 1996). Conversely, human NQO1 utilizes NADH and NADPH with a similar rate, whereas human NQO2 prefers ribosyl, alkyl or phenyl dihydronicotinamides as substrates (Foster *et al.*, 1999; Tedeschi *et al.*, 1995; Zhao *et al.*, 1997). Observations from the structure of rat NQO1–$NADP^+$ showed that a hydrogen bond was formed between the 2′-phosphate of $NADP^+$ and the additional C-terminal domain, which may explain the substrate-selection mechanism (Li *et al.*, 1995). However, the characterized bacterial MdaBs (Wang & Maier, 2004; Hong *et al.*, 2008; Hayashi *et al.*, 1996) and SmMdaB as reported here can specifically select NADPH as a substrate, although these proteins do not have a C-terminal domain. It may be physiologically significant that the bacterial MdaB specifically utilizes NADPH as a substrate, as the NADH/NAD^+ ratio is usually low and the NADPH/$NADP^+$ ratio is usually high in cells, and the specific selection of NADPH as a substrate allows the enzyme to exert its function efficiently. The protein interacts with menadione mainly through non-specific hydrophobic interactions, suggesting that other quinones, such as anthraquinone, may also be substrates of SmMdaB. As an important antioxidation enzyme, structural and biochemical study of SmMdaB should provide critical insights into future drug design against *S. mutans*.

We thank the beamline staff at Photon Factory, KEK, Japan for help in data collection and Xiaoxia Yu at the Institute of Biophysics, Chinese Academy of Sciences for performing the ultracentrifugation assay. This work was supported by grants from the National Basic Research Program of China 973 (No. 2011CB911103 to X-DS) and the National Natural Science Foundation of China (No. 30530190).

References

Adams, P. D., Grosse-Kunstleve, R. W., Hung, L.-W., Ioerger, T. R., McCoy, A. J., Moriarty, N. W., Read, R. J., Sacchettini, J. C., Sauter, N. K. & Terwilliger, T. C. (2002). *Acta Cryst.* D**58**, 1948–1954.
Adams, M. A. & Jia, Z. (2005). *J. Biol. Chem.* **280**, 8358–8363.
Adams, M. A. & Jia, Z. (2006). *J. Mol. Biol.* **359**, 455–465.
Ajdić, D. *et al.* (2002). *Proc. Natl Acad. Sci. USA*, **99**, 14434–14439.
Bateman, A., Coin, L., Durbin, R., Finn, R. D., Hollich, V., Griffiths-Jones, S., Khanna, A., Marshall, M., Moxon, S., Sonnhammer, E. L., Studholme, D. J., Yeats, C. & Eddy, S. R. (2004). *Nucleic Acids Res.* **32**, D138–D141.
Beyer, R. E., Segura-Aguilar, J., di Bernardo, S., Cavazzoni, M., Fato, R., Fiorentini, D., Galli, M. C., Setti, M., Landi, L. & Lenaz, G. (1997). *Mol. Aspects Med.* **18**, S15–S23.
Binter, A., Staunig, N., Jelesarov, I., Lohner, K., Palfey, B. A., Deller, S., Gruber, K. & Macheroux, P. (2009). *FEBS J.* **276**, 5263–5274.
Burley, S. K. & Petsko, G. A. (1986). *FEBS Lett.* **203**, 139–143.
Chatterjee, P. K. & Sternberg, N. L. (1995). *Proc. Natl Acad. Sci. USA*, **92**, 8950–8954.
Chen, S., Wu, K. & Knox, R. (2000). *Free Radic. Biol. Med.* **29**, 276–284.
Emsley, P. & Cowtan, K. (2004). *Acta Cryst.* D**60**, 2126–2132.
Foster, C. E., Bianchet, M. A., Talalay, P., Zhao, Q. & Amzel, L. M. (1999). *Biochemistry*, **38**, 9881–9886.
Georgellis, D., Kwon, O. & Lin, E. C. C. (2001). *Science*, **292**, 2314–2316.
Hayashi, M., Hasegawa, K., Oguni, Y. & Unemoto, T. (1990). *Biochim. Biophys. Acta*, **1035**, 230–236.
Hayashi, M., Ohzeki, H., Shimada, H. & Unemoto, T. (1996). *Biochim. Biophys. Acta*, **1273**, 165–170.
Holm, L. & Rosenström, P. (2010). *Nucleic Acids Res.* **38**, W545–W549.
Hong, Y., Wang, G. & Maier, R. J. (2008). *Microb. Pathog.* **44**, 169–174.
Kwiek, J. J., Haystead, T. A. J. & Rudolph, J. (2004). *Biochemistry*, **43**, 4538–4547.
Li, R., Bianchet, M. A., Talalay, P. & Amzel, L. M. (1995). *Proc. Natl Acad. Sci. USA*, **92**, 8846–8850.
Otwinowski, Z. & Minor, W. (1997). *Methods Enzymol.* **276**, 307–326.
Tedeschi, G., Chen, S. & Massey, V. (1995). *J. Biol. Chem.* **270**, 1198–1204.
Vagin, A. & Teplyakov, A. (2010). *Acta Cryst.* D**66**, 22–25.
Walter, T. S., Meier, C., Assenberg, R., Au, K. F., Ren, J., Verma, A., Nettleship, J. E., Owens, R. J., Stuart, D. I. & Grimes, J. M. (2006). *Structure*, **14**, 1617–1622.
Wang, G. & Maier, R. J. (2004). *Infect. Immun.* **72**, 1391–1396.
Winger, J. A., Hantschel, O., Superti-Furga, G. & Kuriyan, J. (2009). *BMC Struct. Biol.* **9**, 7.
Wu, K., Knox, R., Sun, X. Z., Joseph, P., Jaiswal, A. K., Zhang, D., Deng, P. S.-K. & Chen, S. (1997). *Arch. Biochem. Biophys.* **347**, 221–228.
Zhao, Q., Yang, X. L., Holtzclaw, W. D. & Talalay, P. (1997). *Proc. Natl Acad. Sci. USA*, **94**, 1669–1674.